Supporting Information

Engineering a Zinc Anode Interphasial Chemistry for Acidic, Alkaline and Non-aqueous Electrolytes

Lin Ma[a,b,c]§*, Travis P. Pollard[a]§, Marshall A. Schroeder[a]*, Chao Luo[d], Ye Zhang[e], Glenn Pastel[a], Longsheng Cao[f], Jiaxun Zhang[f], Vadim Shipitsyn[b,c], Yan Yao[e], Chunsheng Wang[f], Oleg Borodin[a]*, Kang Xu[a, g]*

a. Battery Sciences Branch, Energy Science Division, Army Research Directorate, DEVCOM Army Research Laboratory, Adelphi, MD 20783, USA
b. Department of Mechanical Engineering and Engineering Science, University of North Carolina at Charlotte, NC 28220 USA
c. Battery Complexity, Autonomous Vehicle and Electrification (BATT CAVE) Research Center, University of North Carolina at Charlotte, NC 28220 USA
d. Department of Chemical, Environmental and Materials Engineering, University of Miami, Coral Gables, FL, 33146, USA
e. Department of Electrical & Computer Engineering and Texas Center for Superconductivity at the University of Houston, University of Houston, Houston, TX 77204, USA
f. Department of Chemical and Biomolecular Engineering, University of Maryland, College Park, MD, USA
g. Current Affiliation: SES AI, Woburn, MA 01801, USA

§ these authors contributed equally
*Corresponding authors: l.ma@charlotte.edu; marshall.a.schroeder.civ@army.mil; oleg.a.borodin.civ@army.mil; kang.xu@ses.ai

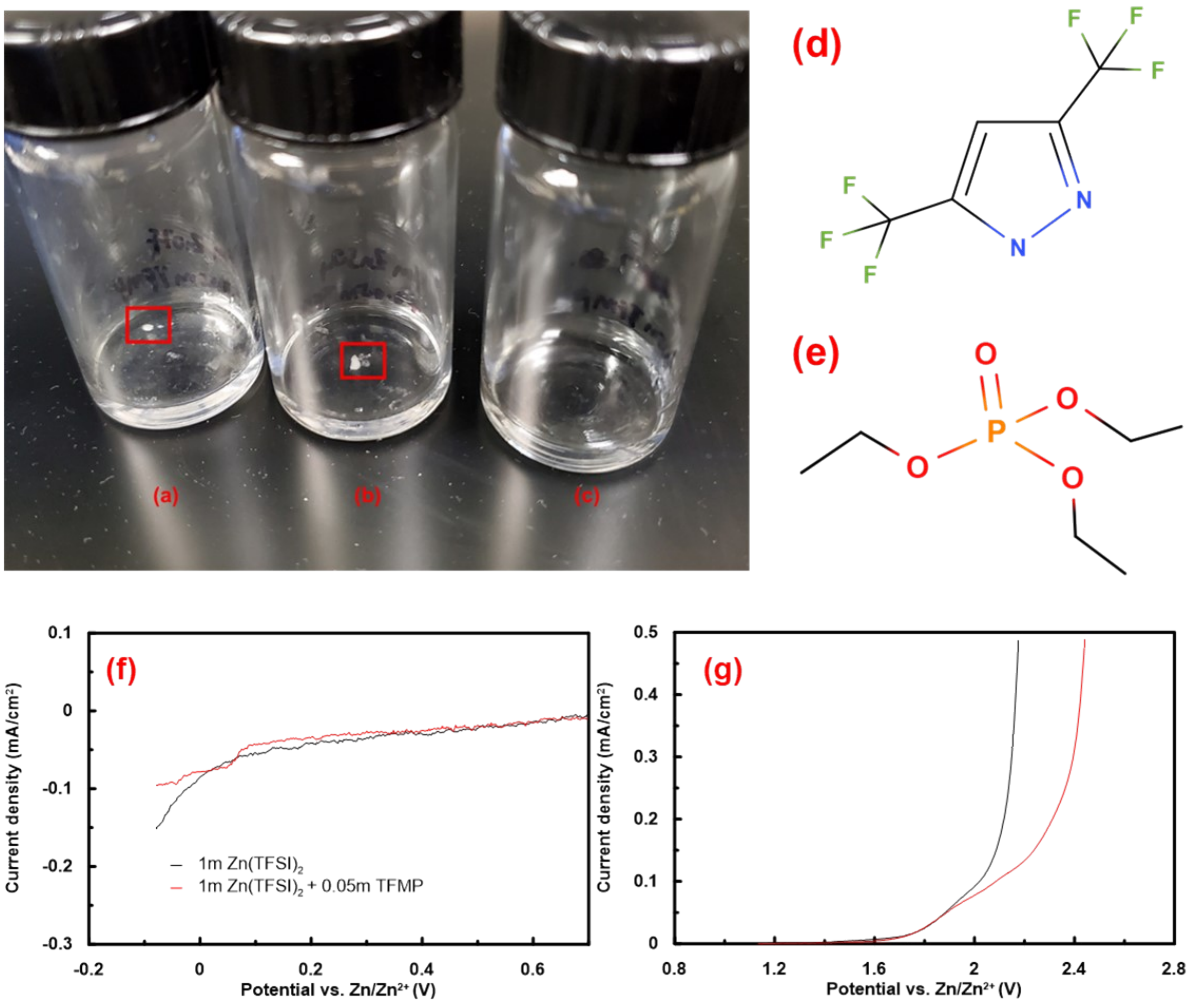

Figure S1. Solubility testing of TFMP (to accelerate the dissolution process, heating at 50°C is necessary) in different aqueous electrolytes: (a) 1m $Zn(OTf)_2$ + 0.05m TFMP in H_2O; (b) 1m $ZnSO_4$ + 0.05m TFMP in H_2O; (c) 1m $Zn(TFSI)_2$ + 0.05m TFMP in H_2O. Red squares indicate the undissolved TFMP in the electrolytes. Chemical structures of TFMP (d) and TEP (e). Electrochemical stability analysis of the aqueous Zn electrolytes including (f) cathodic region and (g) anodic region during 4th cycle. A three electrode Swagelok cell containing stainless steel (SS) as the working electrode, carbon black as the counter electrode and Ag/AgCl as the reference electrode was used for tesing at a scan rate of 5mV/s at room temperature.

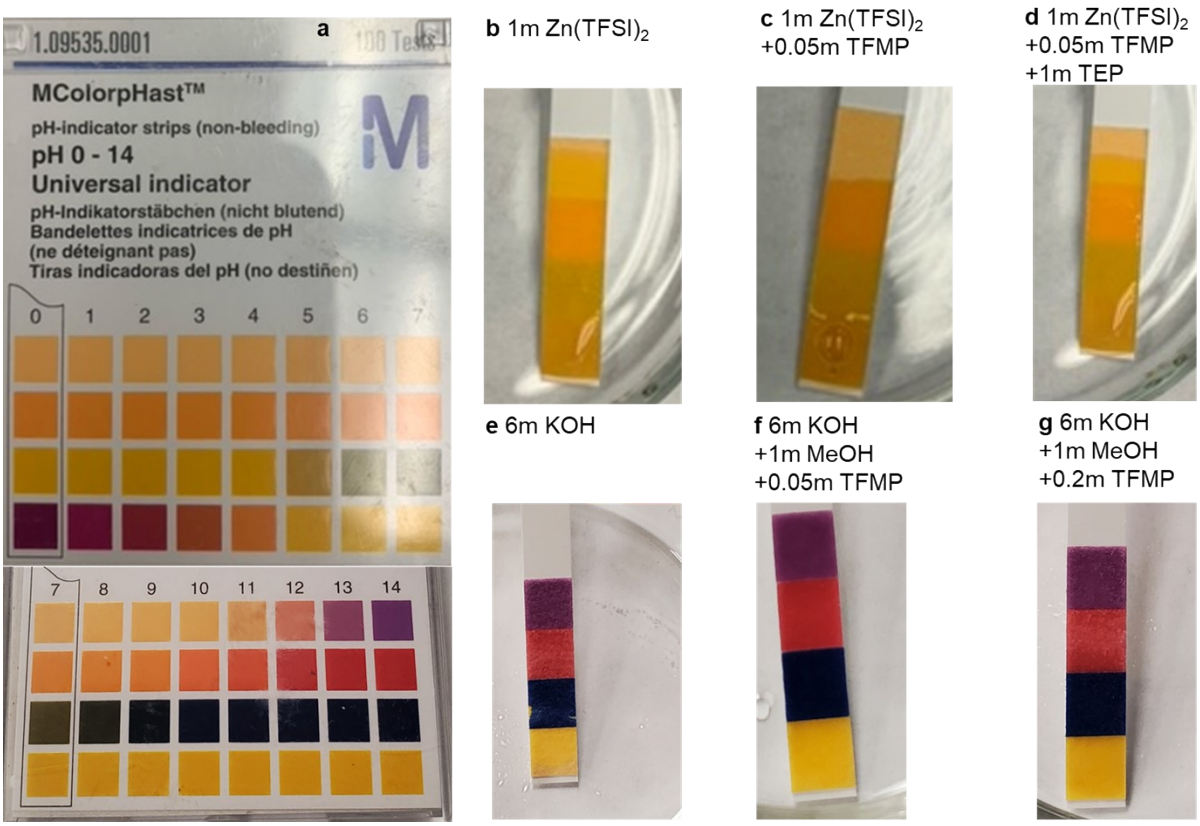

Figure S2. pH paper (a) testing results for different electrolytes: (b) 1m $Zn(TFSI)_2$ in H_2O; (c) 1m $Zn(TFSI)_2$ + 0.05m TFMP in H_2O, (d) 1m $Zn(TFSI)_2$ + 0.05m TFMP + 1m TEP in H_2O, (e) 6m KOH in H_2O, (f) 6m KOH + 1m MeOH + 0.05m TFMP in H_2O and (g) 6m KOH + 1m MeOH + 0.2m TFMP in H_2O.

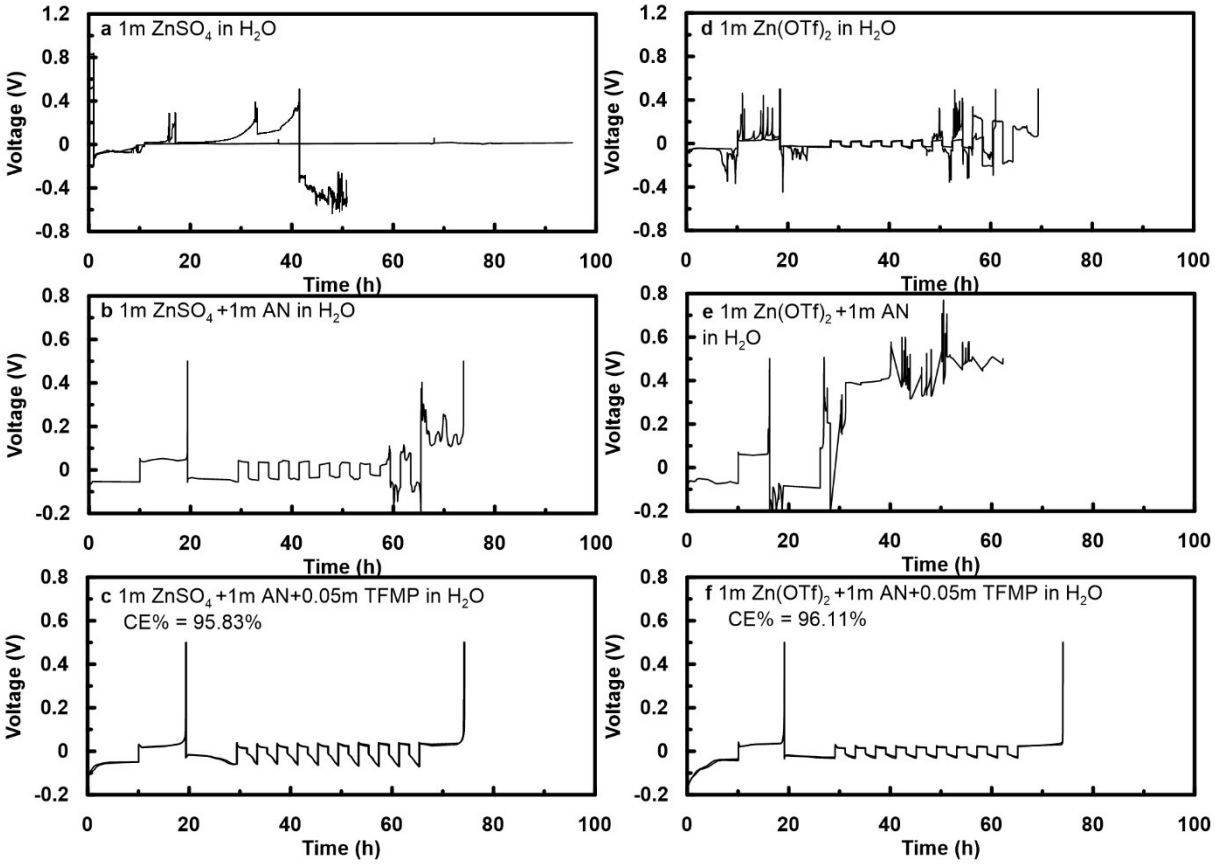

Figure S3. Voltage vs time for Cu|Zn cells at 25°C with different electrolytes: (a) 1m $ZnSO_4$ in H_2O; (b) 1m $ZnSO_4$ +1m AN in H_2O; (c) 1m $ZnSO_4$ +1m AN + 0.05m TFMP in H_2O (d) 1m $Zn(OTf)_2$ in H_2O (e) 1m $Zn(OTf)_2$ + 1m AN in H_2O, and (f) 1m $Zn(OTf)_2$ + 1m AN + 0.05m TFMP in H_2O. Cu was conditioned by plating (0.5 mA/cm^2, 5 mAh/cm^2) and stripping Zn (0.5 V) during the first cycle. Then a Zn reservoir with a capacity of 5 mAh/cm^2 was built on the Cu substrate using 0.5 mA/cm^2. 0.5 mA/cm^2 was used for stripping and plating Zn during the following 9 cycles. A capacity of 1mAh/cm^2 Zn was plated or stripped in each cycle. The cell was charged to 0.5 V to strip Zn during the last step.

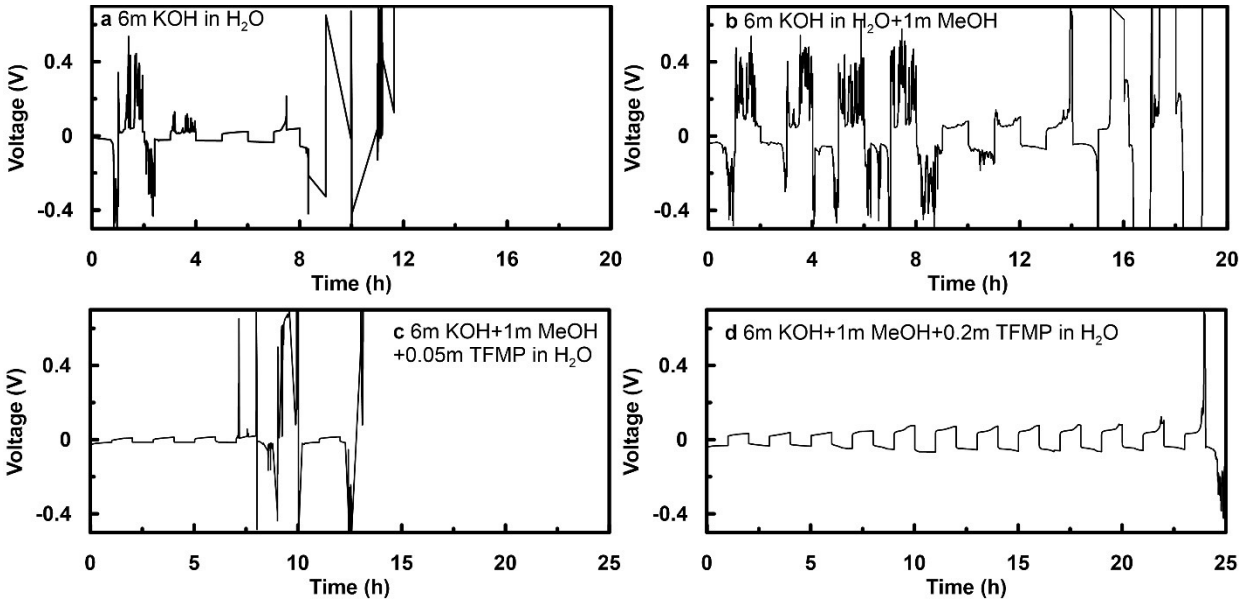

Figure S4. Voltage vs time for Zn|Zn cells (0.5 mA cm^{-2} ,0.5 mAh cm^{-2} per cycle) at 25°C with different electrolytes: (a) 6m KOH in H_2O, (b) 6m KOH+1m MeOH in H_2O, (c) 6m KOH+1m MeOH+0.05m TFMP in H_2O and (d) 6m KOH+1m MeOH+0.2m TFMP in H_2O.

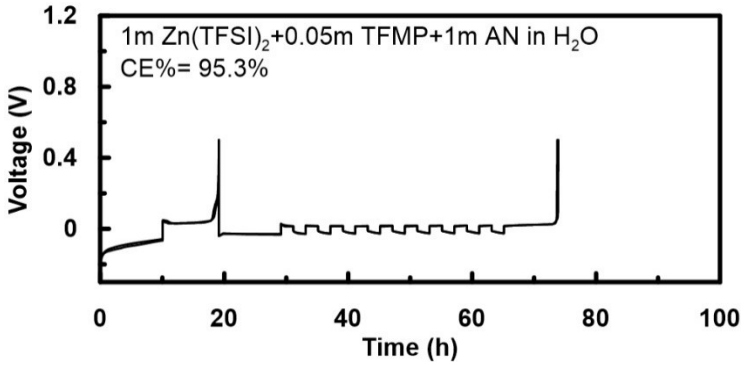

Figure S5. Voltage vs time for Cu|Zn cells at 25°C with 1m $Zn(TFSI)_2$ + 1m AN + 0.05m TFMP in H_2O. Cu was conditioned by plating (0.5 mA/cm^2, 5 mAh/cm^2) and stripping Zn (0.5 V) during the first cycle. Then a Zn reservoir with a capacity of 5 mAh/cm^2 was built on the Cu substrate using 0.5 mA/cm^2. 0.5 mA/cm^2 was used for stripping and plating Zn during the following 9 cycles. A capacity of 1mAh/cm^2 Zn was plated or stripped in each cycle. The cell was charged to 0.5 V to strip Zn during the last step.

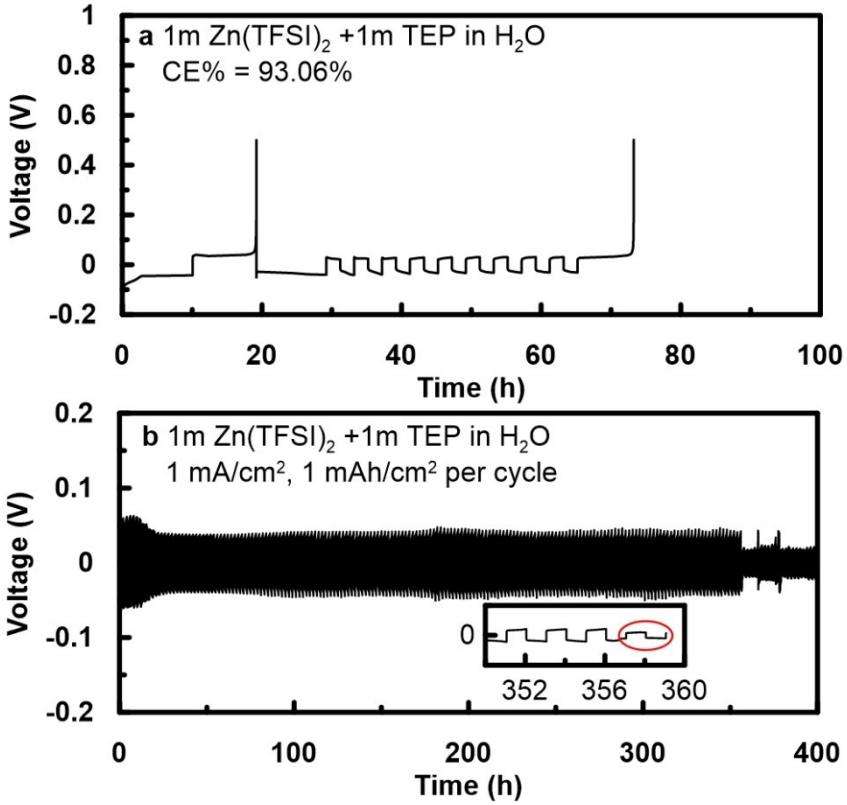

Figure S6. Voltage vs time for (a) Cu|Zn cells and (b) Zn|Zn cells at 25°C with electrolyte of 1m $Zn(TFSI)_2$ + 1m TEP in H_2O. Cu was conditioned by plating (0.5 mA/cm^2, 5 mAh/cm^2) and stripping Zn (0.5 V) during the first cycle. Then a Zn reservoir with a capacity of 5 mAh/cm^2 was built on the Cu substrate by using the same current density used for the following cycling. Different current density (i.e. 0.25 mA/cm^2, 0.5 mA/cm^2, 1mA/cm^2 and 2.5 mA/cm^2) was used for stripping and plating Zn during the following 9 cycles. A capacity of 1mAh/cm^2 (Q_c) Zn was plated or stripped in each cycle. In the final step, a capacity was observed when plated Zn was stripped by charging to 0.5 V. The red circle in (b) suggests cell short circuit.

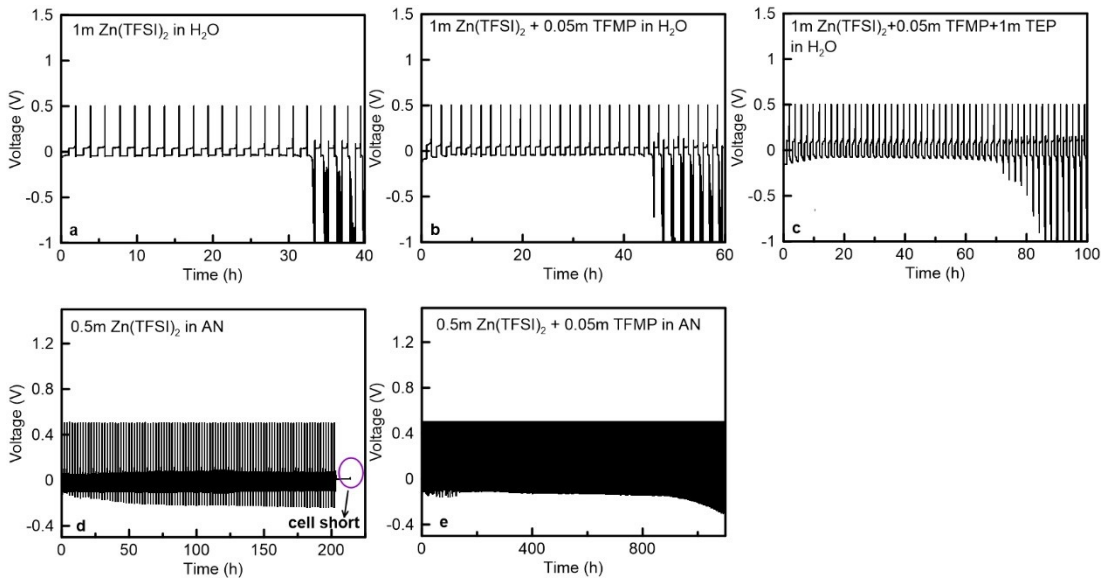

Figure S7. Voltage vs time for Cu|Zn (10 μm) cells (during each cycle 1.17 mA/cm^2, 1.17 mAh/cm^2 (20% Zn utilization) were used to plate Zn on Cu substrate, then charged to 0.5 V to strip Zn) at room temperature with different electrolytes: (a) 1m $Zn(TFSI)_2$ in H_2O; (b) 1m $Zn(TFSI)_2$ + 0.05m TFMP in H_2O; (c) 1m $Zn(TFSI)_2$ + 0.05m TFMP + 1m TEP in H_2O; (d) 0.5m $Zn(TFSI)_2$ in AN; (e) 0.5m $Zn(TFSI)_2$ + 0.05m TFMP in AN. Corresponding CE for (a) has been shown in Figure 1.

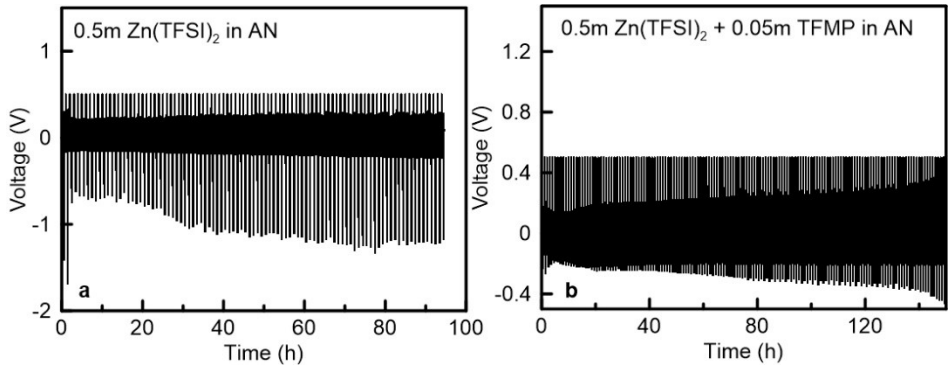

Figure S8. Voltage vs time for Cu|Zn (10 mm) cells (during each cycle 9.36 mA/cm^2, 4.68 mAh/cm^2 (80% Zn utilization) were used to plate Zn on Cu substrate, then charged to 0.5 V to strip Zn) at room temperature with different electrolytes: (a) 0.5m $Zn(TFSI)_2$ in AN; (b) 0.5m $Zn(TFSI)_2$ + 0.05m TFMP in AN. Corresponding CE for (a) has been shown in Figure 1.

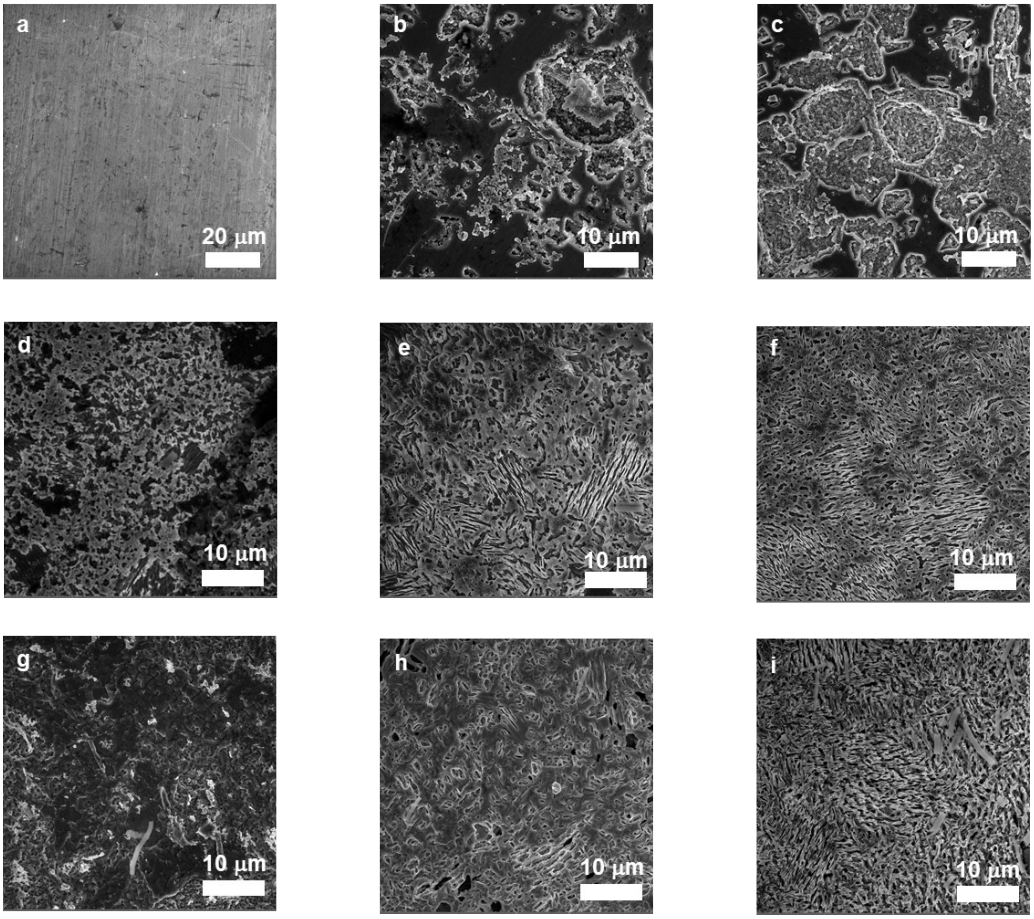

Figure S9. (a) SEM images of Zn metal anode (100 μm) before cycling and after 10 h room temperature cycling (b-i) obtained from Zn|Zn symmetric cells at zero state of charge with different electrolytes: (b) 0.5m $Zn(TFSI)_2$ in AN, (c) 0.5m $Zn(TFSI)_2$ + 0.05m TFMP in AN, (d, g) 1m $Zn(TFSI)_2$ in H_2O, (e, h) 1m $Zn(TFSI)_2$ + 0.05m TFMP in H_2O, (f, i) 1m $Zn(TFSI)_2$ + 0.05m TFMP + 1m TEP in H_2O. Different cycling conditions were used: (d-f) 0.5 mA cm^{-2}, 0.5 mAh cm^{-2} per cycle, (b-c, g-i) 2.5 mA cm^{-2}, 2.5 mAh cm^{-2} per cycle.

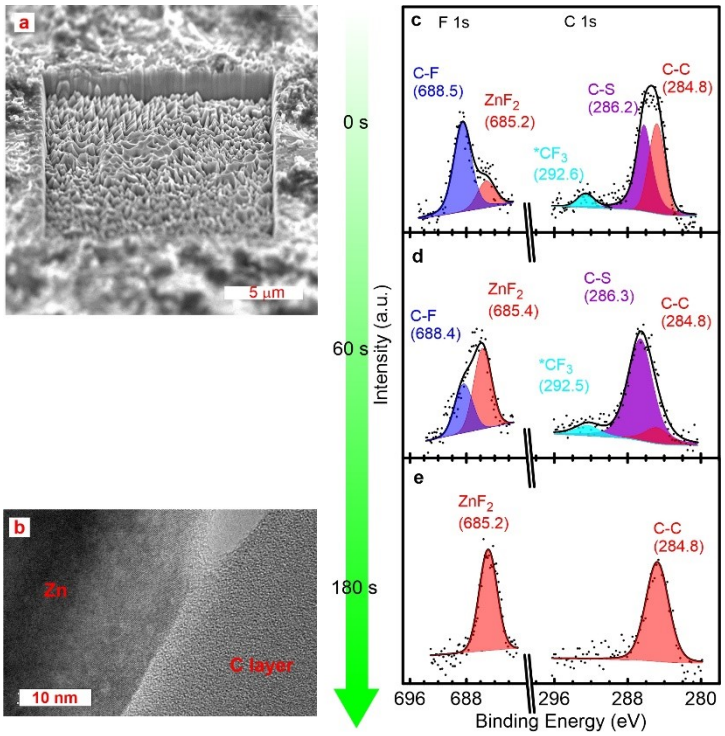

Figure S10. Zn metal anode morphology and SEI information after 10 h cycling (Zn|Zn cell setup, 0.5 mA cm^{-2}, 0.5 mAh cm^{-2} per cycle) at room temperature with 1m $Zn(TFSI)_2$ in H_2O. Zn morphology was obtained using FIB-SEM (**a**). SEI information was obtained using TEM (**b**) and depth profile XPS (**c-e**).

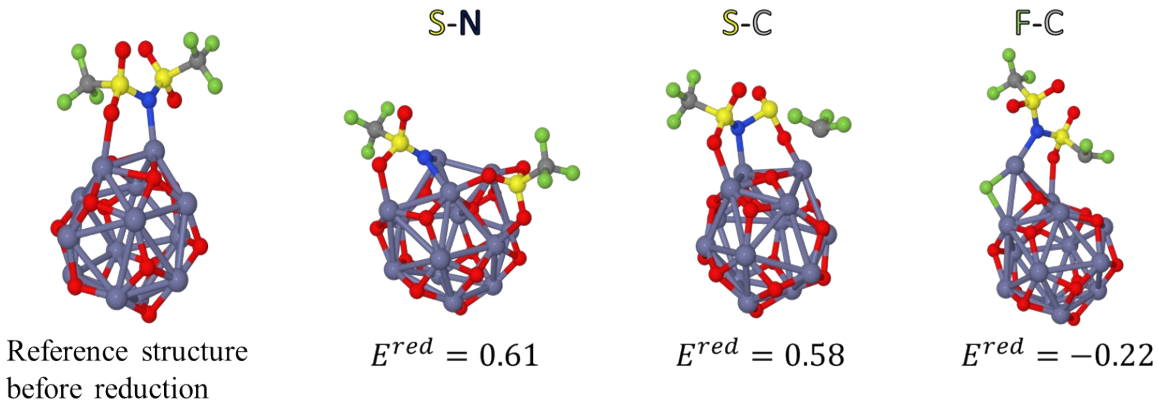

Figure S11. Computed reduction potentials from DFT for the decomposition of a $[ZnTFSI]^+$ species on a nano-scale ZnO cluster $(ZnO)_{12}$ which might be present on the Zn metal surface. The calculated reduction potential is in V vs. Zn^{2+}/Zn and labeled in the Figure. Decomposition of the $TFSI^-$ anion on a neutral $(ZnO)_{12}$ cluster results in potentials of 0.13 V, -0.17 V, and -1.00 V for S-N, S-C, and F-C cleavage products, respectively.

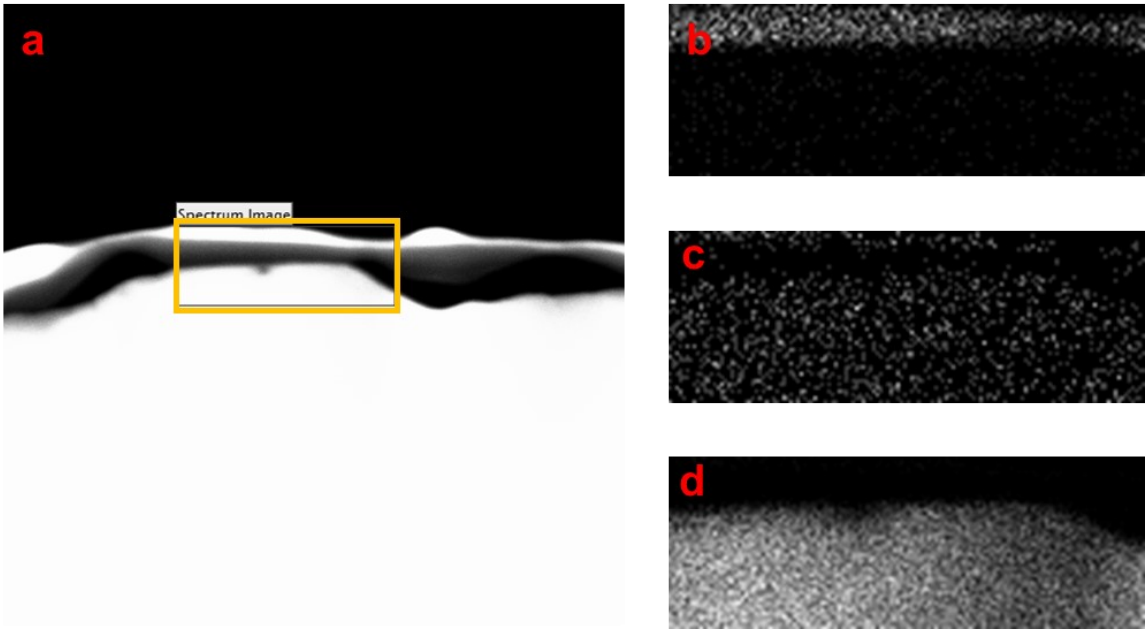

Figure S12. (a) STEM HAADF mode observation of Zn metal with the evolved interphase layer. STEM EDS mapping area is indicated by the yellow rectangular box. (b-d) EDS mapping of C (b), F (c) and Zn (d). Zn sample was obtained from Zn|Zn cells with 1m $Zn(TFSI)_2$+0.05m TFMP in H_2O after 10h cycling (0.5 mA/cm^2, 0.5 mAh/cm^2) at zero state of charge.

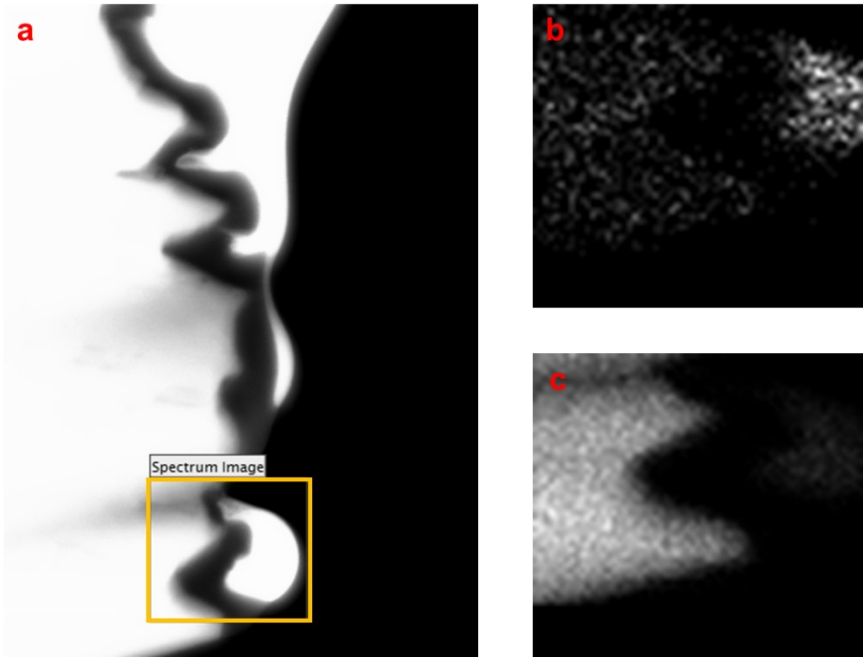

Figure S13. (a) STEM HAADF mode observation of Zn metal with the evolved interphase layer. STEM EDS mapping area is indicated by the yellow rectangular box. (b-c) EDS mapping of F (b), and Zn (c). Zn sample was obtained from Zn|Zn cells with 1m $Zn(TFSI)_2$+0.05m TFMP+1m TEP in H_2O after 10h cycling (0.5 mA/cm^2, 0.5 mAh/cm^2) at zero state of charge.

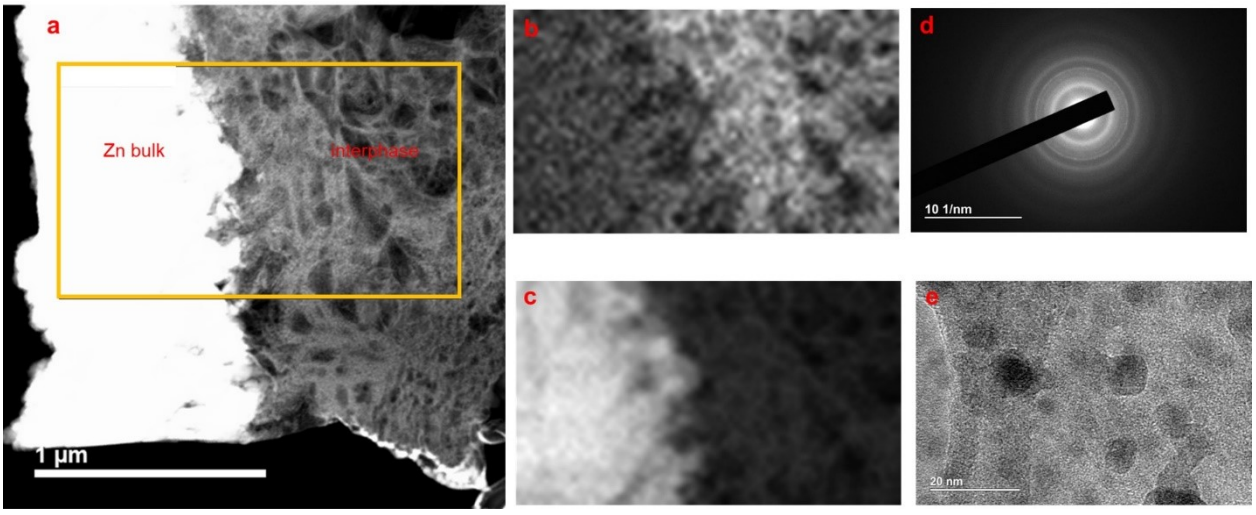

Figure S14. (a) STEM HAADF mode observation of Zn metal with the evolved interphase layer. STEM EDS mapping area is indicated by the yellow rectangular box. (b-c) EDS mapping of F (b), and Zn (c). (d) Selected-area electron diffraction of the interphase region in (a). (e) High resolution TEM image of the interphase region in (a). Zn sample was obtained from Zn|Zn cells with 1m $Zn(TFSI)_2$+0.05m TFMP in H_2O after 200h cycling (0.5 mA/cm^2, 0.5 mAh/cm^2) at zero state of charge.

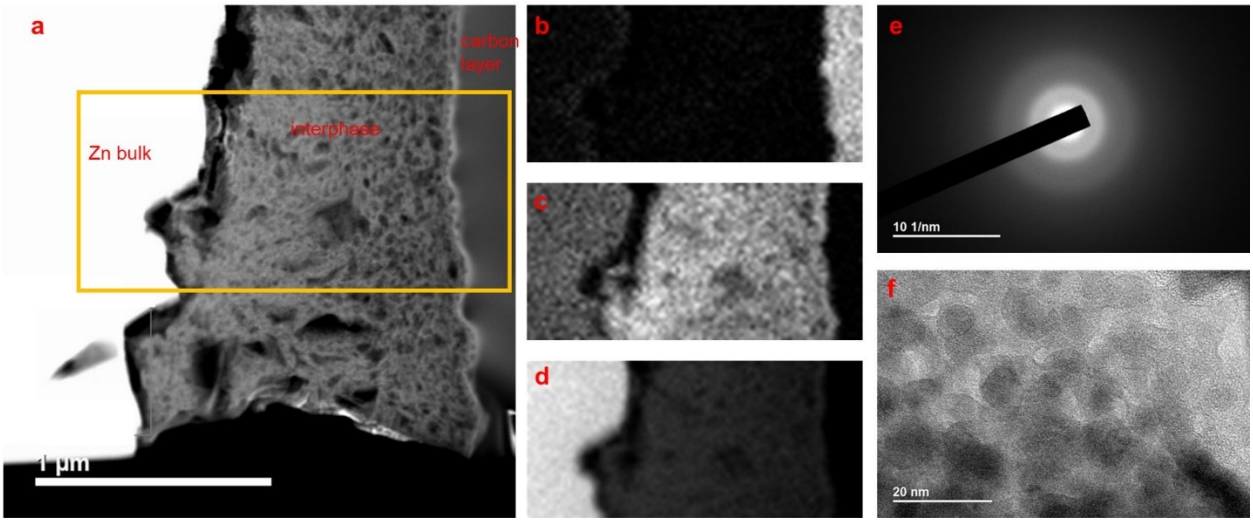

Figure S15. (a) STEM HAADF mode observation of Zn metal with the evolved interphase layer. STEM EDS mapping area is indicated by the yellow rectangular box. (b-d) EDS mapping of C (b), F (c), and Zn (d). (e) Selected-area electron diffraction of the interphase region in (a). (f) High resolution TEM image of the interphase region in (a). Zn sample was obtained from Zn|Zn cells with 1m $Zn(TFSI)_2$+0.05m TFMP+1m TEP in H_2O after 200h cycling (0.5 mA/cm^2, 0.5 mAh/cm^2) at zero state of charge.

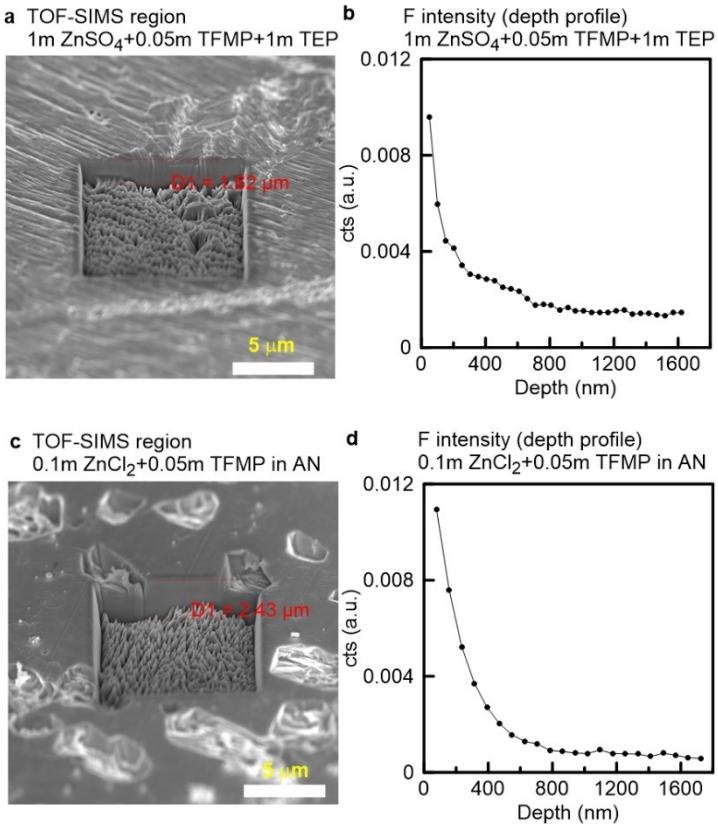

Figure S16. FIB-SEM images (a, c) and corresponding fluorine signal intensity depth profile (b, d) during time of flight secondary ion mass spectrometry (ToF-SIMS) analysis on the Zn metal anodes obtained from Zn|Zn symmetric cells at zero state of charge after 10h cycling (0.5 mA/cm^2, 0.5 mAh/cm^2) at room temperature using different electrolytes: (a-b) 1m $ZnSO_4$ + 0.05m TFMP + 1m TEP in H_2O; (c-d) 0.1m $ZnCl_2$ + 0.05m TFMP in AN.

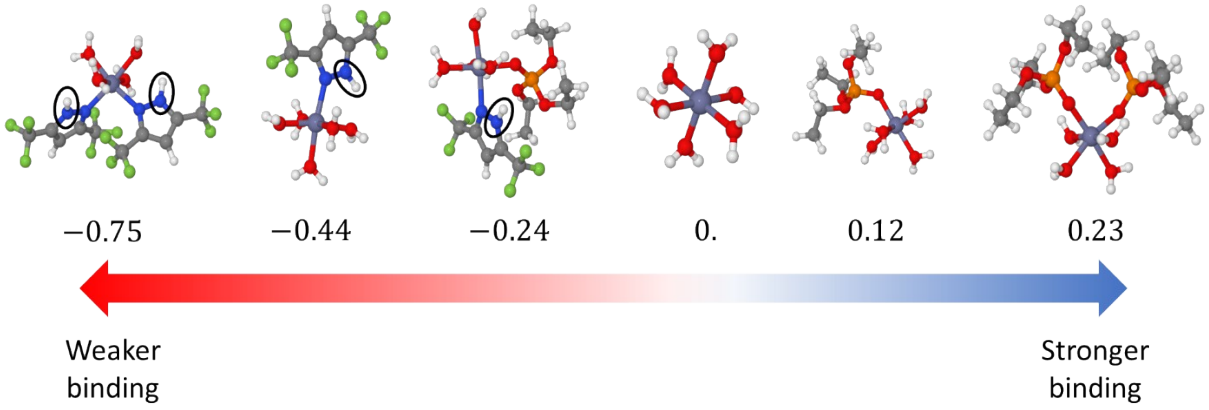

Figure S17. Binding free energies from density functional theory relative to $Zn(H_2O)_6$ in eV for various solvates comprising Zn, H_2O, TEP, and TFMP. Values >0 eV indicate stronger binding than $Zn(H_2O)_6$. The N-H protons are highlighted by ovals on the left-hand side of this figure.

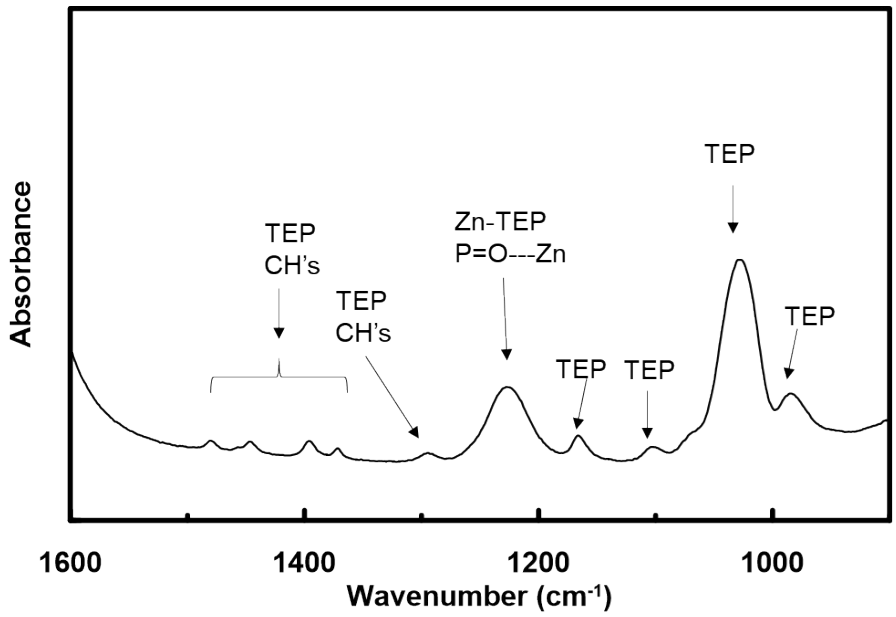

Figure S18. IR spectrum of 1m $ZnCl_2$ +1m TEP in H_2O.

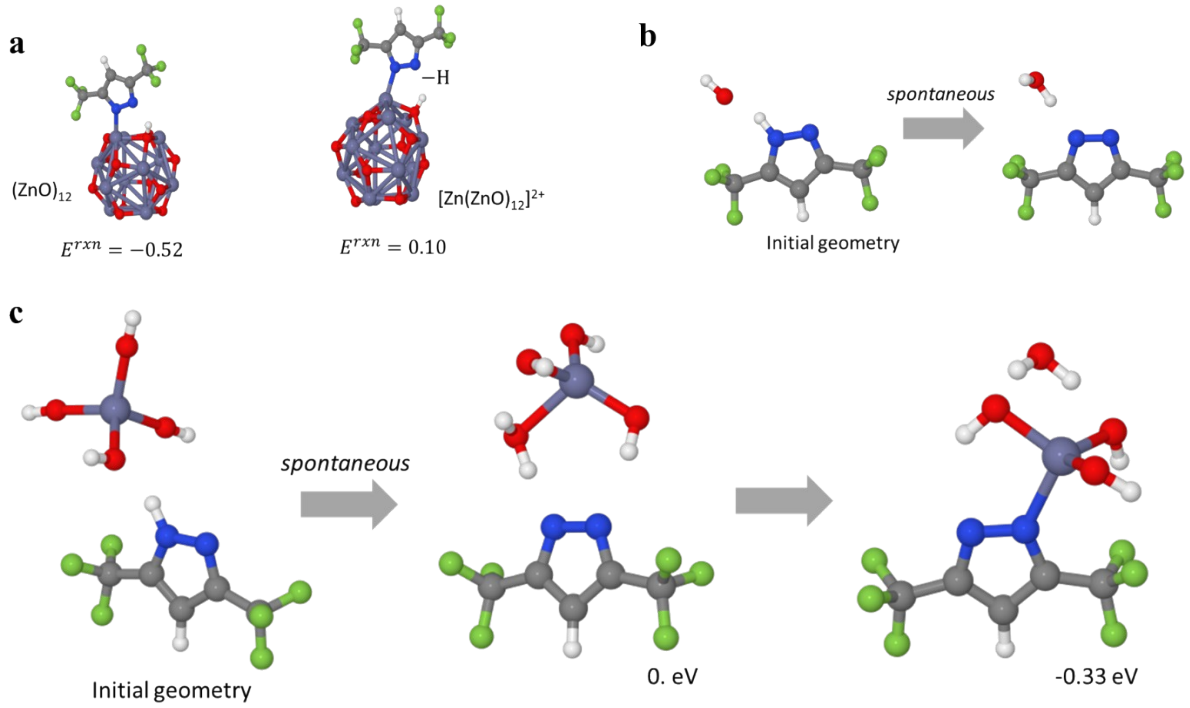

Figure S19. Computed reaction free energies in eV to deprotonate TFMP (a) on a neutral and charged ZnO nanoparticle, (b) with OH^- anions, (c) with $[Zn(OH)_4]^{2-}$. In (c), TFMP-H displaces the reformed water molecule and has a free energy 0.33 eV lower than that of the middle structure with water still in the first solvation shell (meaning, it is favorable for the anion to displace the water). Structures labeled 'initial geometry' are optimized with the non-reactive Merck94 force field so the proton does not initially transfer. Where labeled 'spontaneous', the initial geometry during optimization with DFT converges on a geometry with the proton transferred. It's an entirely energetically 'downhill' process.

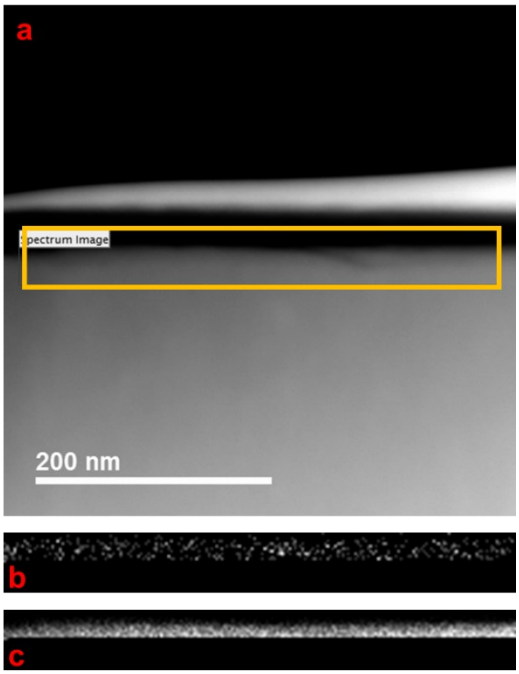

Figure S20. (a) STEM HAADF mode observation of Zn metal with the evolved interphase layer. STEM EDS mapping area is indicated by the yellow rectangular box. (b-c) EDS mapping of F (b), and Zn (c). Zn sample was obtained from Zn|Zn cells with 0.5m $Zn(TFSI)_2$+0.05m TFMP in AN after 10h cycling (0.5 mA/cm^2, 0.5 mAh/cm^2) at zero state of charge.

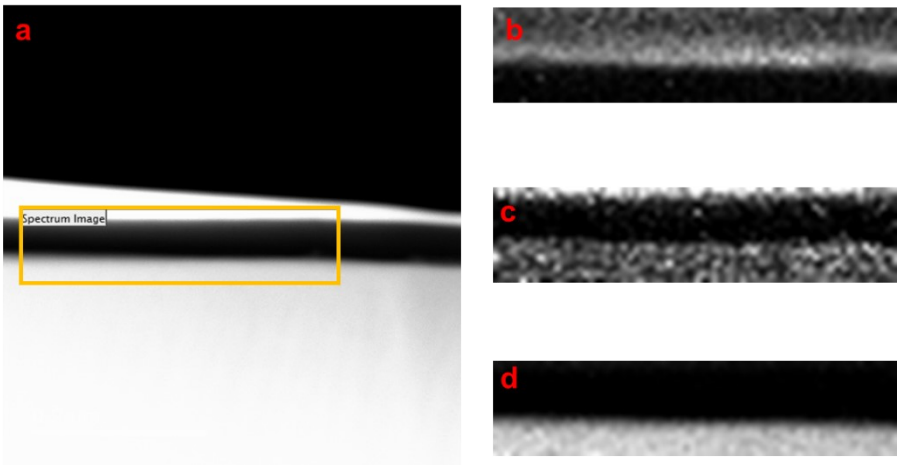

Figure S21. (a) STEM HAADF mode observation of Zn metal with the evolved interphase layer. STEM EDS mapping area is indicated by the yellow rectangular box. (b-d) EDS mapping of C (b), F (c), and Zn (d). Zn sample was obtained from Zn|Zn cells with 0.5m $Zn(TFSI)_2$+0.05m TFMP in AN after 200h cycling (0.5 mA/cm^2, 0.5 mAh/cm^2) at zero state of charge.

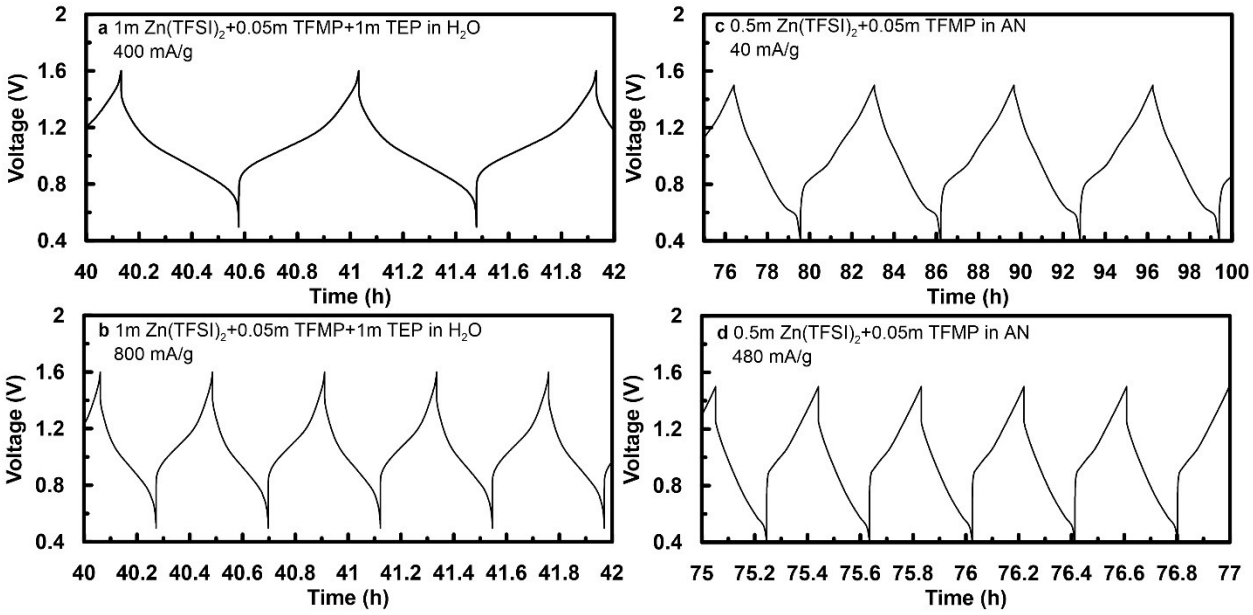

Figure S22. Voltage vs time for PBQS|Zn (10 μm) and PANI|Zn (10 μm) during long term cycling at 30°C with different electrolytes as labeled. Corresponding cycling results have been shown in Figure 5b, e. In Figure S21a, each discharge step takes ~0.5h and corresponding areal capacity will be $400\frac{mA}{g} \times 6\frac{mg}{cm^2} \times 0.5h = 1.2\frac{mAh}{cm^2}$. As a result, Zn utilization percentage per cycle will be $1.2\frac{mAh}{cm^2} \div 5.85\frac{mAh}{cm^2} = 20.5\%$. Zn utilization percentage per cycle for Figure S21b, S21c, and S21d are 16.4%, 18.5%, and 14.8%, respectively, calculated using the same way for Figure S21a.

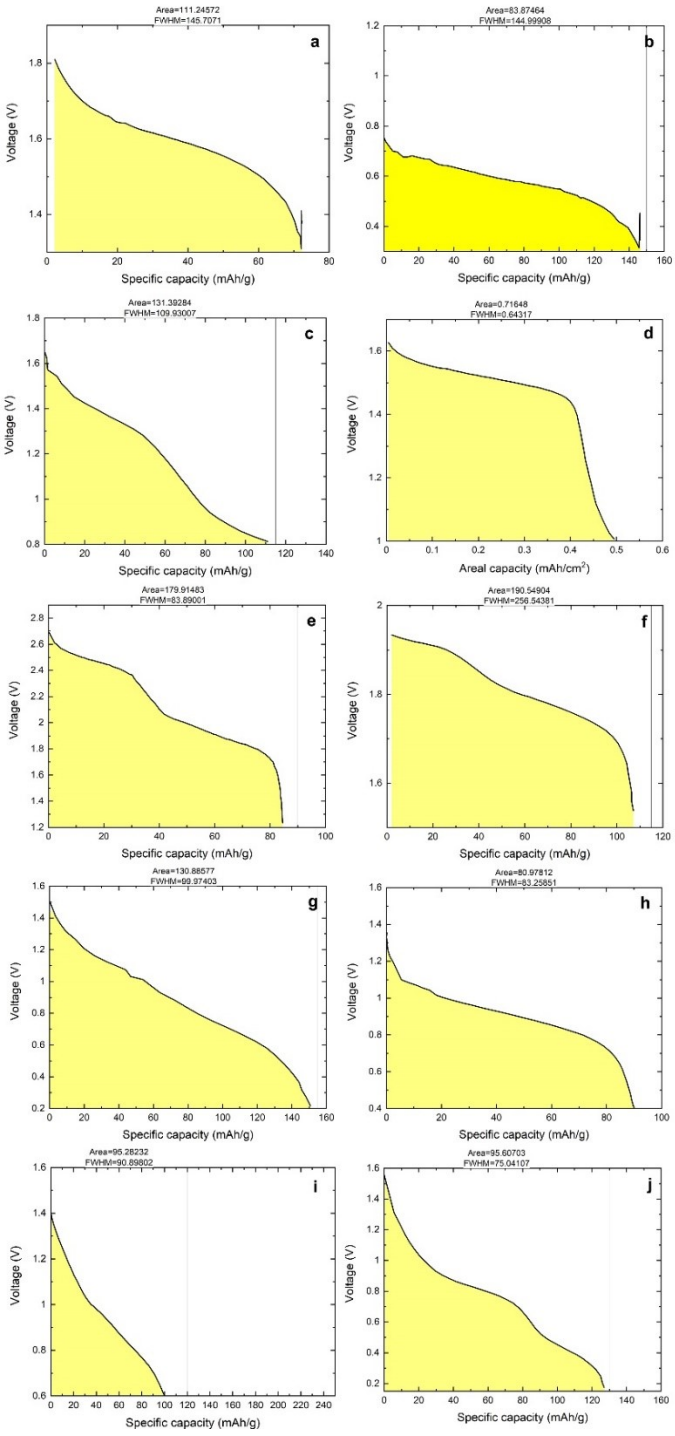

Figure S23. Digitized voltage vs. capacity from reported Zn electrolyte work (2018-2021): (a) 0.5M $Zn(OTf)_2$ in TEP/H_2O (7/3 by vol.)[1]; (b) 0.5M $Zn(OTf)_2$ in TMP/DMC (1/1 by vol.)[2]; (c) 3M $Zn(OTf)_2$+2 vol.% Et_2O in H_2O[3]; (d) 1M $Zn(Ac)_2$+0.4M $Mn(Ac)_2$ in H_2O[4]; (e) $Zn(TFSI)_2$/EMC/TMP 3/5/11 by mol[5]; (f) 30m $ZnCl_2$+5m LiCl in H_2O[6]; (g) 30m $ZnCl_2$+5m LiCl in H_2O[6]; (h) $Zn(ClO_4)_2$•$6H_2O$/SN 1/8 by mol[7]; (i) 2M $ZnSO_4$ in H_2O/MeOH (1/1 by vol)[8]; (j) 1M

$Zn(OTf)_2$+0.025M $Zn(H_2PO_4)_2$ in H_2O[9]. Integrated area is shown in yellow in each panel to calculate average voltage.

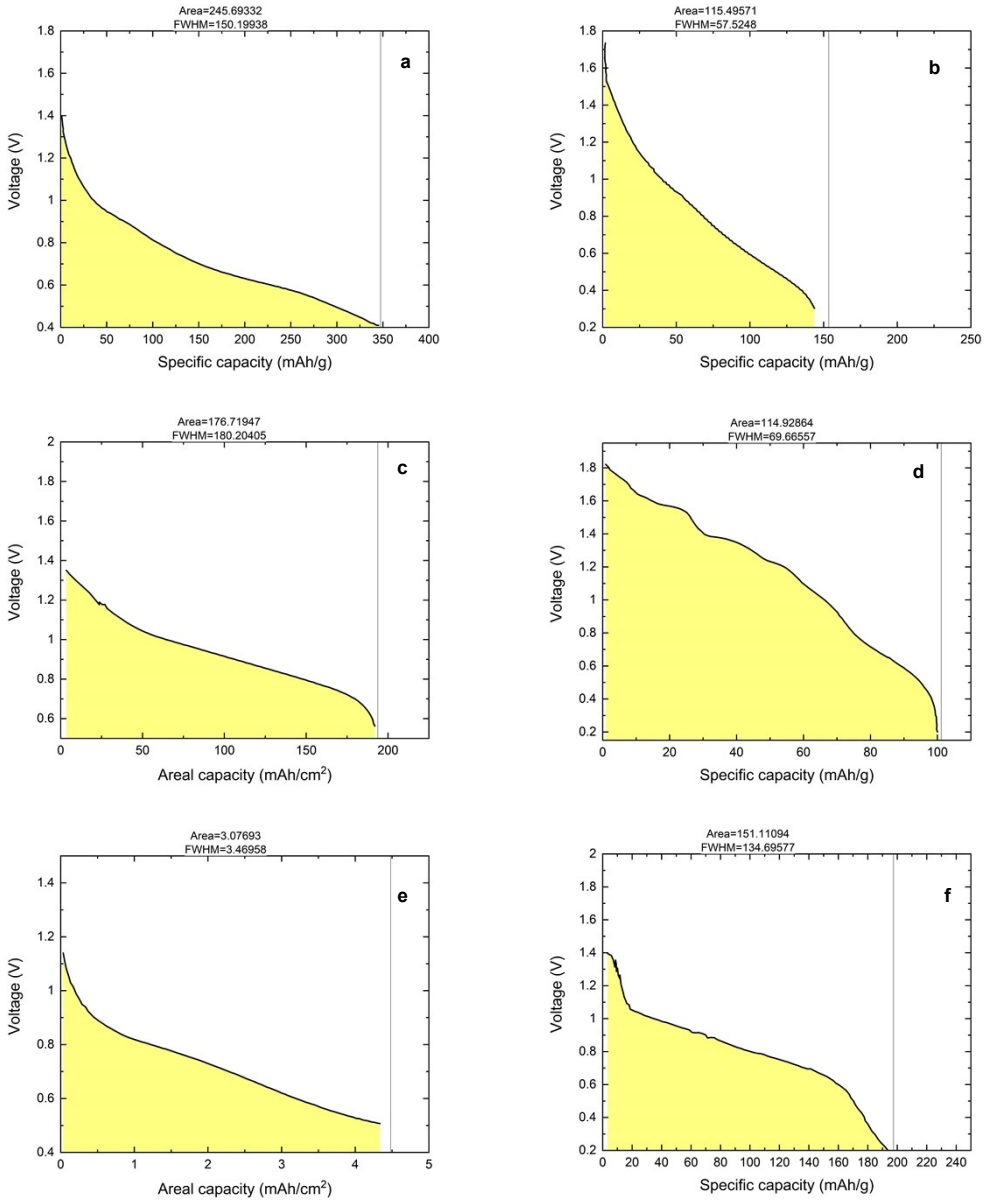

Figure S24. Digitized voltage vs. capacity from reported Zn electrolyte work (2022-2023): (a) $Zn(ClO_4)_2$•$6H_2O$/MSM/H_2O 1.2/3.6/3 by mol[10]; (b) hydrous 4m $Zn(BF_4)_2$ in EG[11]; (c) chitosan[12]; (d) 30m $ZnCl_2$+5m LiCl+10m TMACl in H_2O:DMC (5:1 by mol)[13]; (e) 2mmol $Zn(OTf)_2$ in H_2O/SL (10/7 by wt)[14]; (f) 10m $Zn(Ac)_2$+15m KAc; 10m $Zn(Ac)_2$+24m urea; 8m $Zn(Ac)_2$+30m acetamide[15]. Integrated area is shown in yellow in each panel to calculate average voltage.

Supplementary Table 1. Metrics of interest for previously published rechargeable Zn metal battery electrolyte efforts (2018-2023) corresponding to Figure 5g. Average voltage was obtained by using integration area divided by the capacity in voltage-capacity curve (Figures S23-24), if not directly reported in the literature. The calculation is only based on the volume of cathode and anode. 30% porosity has been considered during the cathode thickness calculation, if the thickness is not reported in the reference.

Ref.	cathode active material and loading	cathode mixture ratio (active material/carbon black/binde	cathode and Zn thickness (μm)	electrolyte	volumetric energy density based on total volume of	voltage range and average voltage	Specific capacity used for energy density estimation	N/P	temperature	note
this work	PBQS, 6 mg cm^{-2}	7/2/1	30 and 10	1m $Zn(TFSI)_2$+1m TEP+0.05m TFMP in H_2O	267.3 Wh L^{-1}	0.5-1.6V, 0.99V	180 mAh g^{-1} (based on cathode)	5.42	30°C	
this work	PANI, 9 mg cm^{-2}	7/2/1	45 and 10	0.5m $Zn(TFSI)_2$+0.05m TFMP in AN	182 Wh L^{-1}	0.4-1.5V, 0.89V	125 mAh g^{-1} (based on cathode)	5.2	30°C	
Wang et al.[16]	$LiMn_2O_4$, unknown	8/1/1	unknown	1m $Zn(TFSI)_2$+20m LiTFSI in H_2O	208 Wh L^{-1}	0.8-2.1V, 1.8V	66 mAh g^{-1} (based on both cathode and anode)	4.43	N/A	N/P mass ratio is 0.8/1, Zn powder mixed with carbon black, PVDF (8/1/1) is used as anode here so 30% porosity is also estimated for anode
Naveed et al.[1]	KCuHCf, 1 mg cm^{-2}	7.5/1/1.5	10.8 and 250	0.5M $Zn(OTf)_2$ in TEP/H_2O (7/3 by vol.)	4.22 Wh L^{-1}	1.3-2V, 1.5V	73.3 mAh g^{-1} (based on cathode)	1995	25°C	
Naveed et al.[2]	VS_2, 4 mg cm^{-2}	7/2/1	34.6 and unknown	0.5M $Zn(OTf)_2$ in TMP/DMC (1/1 by vol.)	51.6 Wh L^{-1} and 17.1 Wh L^{-1}	0.3-1V, 0.57V	102.57 mAh g^{-1} (based on cathode)	14.3 and 143	N/A	Zn thickness is unknown in this work. An estimation of 10 and 100 um was used for Zn to estimate energy density and N/P.
Xu et al.[3]	α-MnO_2, 3.5 mg cm^{-2}	7/2/1	21.1 and unknown	3M $Zn(OTf)_2$+2 vol.% Et_2O in H_2O	135 Wh L^{-1} and 34.7 Wh L^{-1}	0.8-1.8V, 1.2V	100 mAh g^{-1} (based on cathode)	16.7 and 167	N/A	Zn thickness is unknown in this work. An estimation of 10 and 100 um was used for Zn to estimate energy density and N/P.
Zeng et al.[4]	MnO_2, 1.8 mg cm^{-2}	unknown	11 and 100	1M $Zn(Ac)_2$+0.4M $Mn(Ac)_2$ in H_2O	126.1Wh L^{-1}	1-1.8V, 1.4V	1 mAh cm^{-1} (based on cathode)	58.5	N/A	A 7/2/1 slurry ratio in cathode was used to estimate its thickness.
Qiu et al.[17]	V_2O_5, 14.3 mg cm^{-2}	7/2/1	106 and 20	$Zn(TFSI)_2$/acetamide 1/7 by mol	58.7Wh L^{-1}	0.6-1.8V, 1.01V	25.5 mAh g^{-1} (based on both cathode and	7.45	N/A	N/P mass ratio is 1/1.
Zhao et al.[18]	$LiMn_2O_4$, 5 mg cm^{-2}	8/1/1	36.1 and 19.1	LZ-DES/2H_2O	225Wh L^{-1}	1.5-2.1V, 1.92V	110 mAh g^{-1} (based on cathode)	20.3	N/A	
Chen et al.[5]	graphite, 2.3 mg cm^{-2}	8.5/0.5/1	17.6 and 250	$Zn(TFSI)_2$/EMC/TMP 3/5/11 by mol	13.5Wh L^{-1}	1.2-2.8V, 2.1V	75 mAh g^{-1} (based on cathode)	8478	N/A	
Zhang et al.[6]	$LiMn_2O_4$, 6.5 mg cm^{-2}	8/1/1	46.8 and 5.5	30m $ZnCl_2$+5m LiCl in H_2O	233Wh L^{-1}	1.55-1.95V, 1.8V	100 mAh g^{-1} (based on cathode)	4.95	N/A	

Ref.	cathode active material and loading	cathode mixture ratio (active material/carbon black/binde	cathode and Zn thickness (μm)	electrolyte	volumetric energy density based on total volume of	voltage range and average voltage	Specific capacity used for energy density estimation	N/P	temperature	note
Zhang et al.[6]	$V_2O_5•H_2O$, 1.5 mg cm^{-2}	7/2/1	11.3 and 2.5	30m $ZnCl_2$+5m LiCl in H_2O	188.2 Wh L^{-1}	0.2-1.6V, 0.87V	150 mAh g^{-1} (based on cathode)	6.5	N/A	
Yang et al. [7]	PDB, 0.21mg cm^{-2}	6/2/2	2.6 and 0.74	$Zn(ClO_4)_2•6H_2O$/SN 1/8 by mol	50.9 Wh L^{-1}	0.4-1.5V, 0.9V	90 mAh g^{-1} (based on cathode)	22.9	N/A	
Hao et al.[8]	PANI, 10 mg cm^{-2}	N/A(polymerized on current collector)	50 and 10	2M $ZnSO_4$ in H_2O/MeOH (1/1 by vol)	158 Wh L^{-1}	0.6-1.6V, 0.95V	100 mAh g^{-1} (based on cathode)	5.9	room temperature	Cathode thickness is estimated based on the loading proportion of PANI used in this work
Zeng et al.[9]	V_2O_5, 8.7 mg cm^{-2}	7/2/1	64.7 and 10	1M $Zn(OTf)_2$+0.025M $Zn(H_2PO_4)_2$ in H_2O	96.1 Wh L^{-1}	0.2-1.6V, 0.75V	110 mAh g^{-1} (based on cathode)	6.1	N/A	
Han et al.[10]	CaV_4O_9, 1.33 mg cm^{-2}	7/2/1	10 and 80	$Zn(ClO_4)_2•6H_2O$/MSM /H_2O 1.2/3.6/3 by mol	36.7 Wh L^{-1}	0.4-1.6V, 0.71V	350 mAh g^{-1} (based on cathode)	101	N/A	Cathode thickness is estimated based on the loading proportion of CaV_4O_9 used in this work
Han et al.[11]	V_2O_5, 2-3 mg cm^{-2}	7/2/1	22 and 17	Hydrous 4m $Zn(BF_4)_2$ in EG	105.8 Wh L^{-1}	0.2-1.8V, 0.8V	140 mAh g^{-1} (based on cathode)	19.1	N/A	Cathode thickness is estimated based on the loading of 3 mg cm^{-2}
Wu et al.[12]	PBQS, 10 mg cm^{-2}	7/2/1	77 and 100	Chitosan-Zn	99.8 Wh L^{-1}	0.5-1.7V, 0.92V	190 mAh g^{-1} (based on cathode)	30.8	room temperature	Cathode thickness is estimated based on the loading proportion of PBQS used in this work
Jiang et al.[19]	$VOPO_4•2H_2O$, 22.5 mg cm^{-2}	8.75/0.25/1	121 and 1.2	30m $ZnCl_2$+5m LiCl+10m TMACl in H_2O:DMC (5:1 by mol)	202.5 Wh L^{-1}	0.2-1.8V, 1.1V	100 mAh g^{-1} (based on cathode)	2.3	room temperature	Cathode thickness is estimated based on its loading proportion of $VOPO_4•2H_2O$ used in this work
Li et al.[14]	$Zn_{0.25}V_2O_5•nH_2O$ 42.46 mg cm^{-2}	8/1/1	580 and 11	2mmol $Zn(OTf)_2$ in H_2O/SL (10/7 by wt)	52.8 Wh L^{-1}	0.5-1.4V, 0.71V	4.4 mAh cm^{-1} (based on cathode)	1.08	N/A	Cathode thickness is reported by the authors
Dong et al.[15]	PTO, 2 mg cm^{-2}	6/3/1	19 and 3.5	10m $Zn(Ac)_2$+15m KAc; 10m $Zn(Ac)_2$+24m urea; 8m $Zn(Ac)_2$+30m acetamide	133.9 Wh L^{-1}	0.2-1.4V, 0.78V	200 mAh g^{-1} (based on cathode)	5.12	N/A	Cathode thickness is estimated based on the loading proportion of PTO used in this work
Yang et al.[20]	Air	N/A	215 and unknown	$Li_2ZnCl_4•RH_2O$	186 Wh L^{-1} and 127 Wh L^{-1}	1-1.75V, 1V	4 mAh cm^{-1}	N/A	20°C	Cathode thickness is the air electrode. Zn thickness is unknown in this work. An estimation of 10 and 100 um was used for Zn to estimate energy density

PANI: polyaniline; DES: deep eutectic solvents; PDB: poly(2,3-dithiino-1,4-benzoquinone); TMP: triethyl phosphate; TEP: triethyl phosphate; MSM: methylsulfonylmethane; EG: ethylene glycol; PBQS: poly(benzoquinonyl sulfide); DMC: dimethyl carbonate; TMACl: trimethylammonium chloride; SL: sulfolane; PTO: pyrene-4,5,9,10-tetraone

Supplementary Table 2. The ionic conductivity of different electrolytes at room temperature.

Electrolyte	Conductivity (mS/cm)
1m $Zn(TFSI)_2$ in H_2O	36.55
1m $Zn(TFSI)_2$ + 0.05m TFMP in H_2O	36.28
1m $Zn(TFSI)_2$ + 0.05m TFMP + 1m TEP in H_2O	27.95
0.5m $Zn(TFSI)_2$ in AN	33.00
0.5m $Zn(TFSI)_2$ + 0.05m TFMP in AN	32.45

Supplementary references:

1 Naveed, A., Yang, H., Yang, J., Nuli, Y. & Wang, J. Highly Reversible and Rechargeable Safe Zn Batteries Based on a Triethyl Phosphate Electrolyte. *Angewandte Chemie International Edition* **58**, 2760-2764, doi:https://doi.org/10.1002/anie.201813223 (2019).

2 Naveed, A. *et al.* A Highly Reversible Zn Anode with Intrinsically Safe Organic Electrolyte for Long-Cycle-Life Batteries. *Advanced Materials* **31**, 1900668, doi:https://doi.org/10.1002/adma.201900668 (2019).

3 Xu, W. *et al.* Diethyl ether as self-healing electrolyte additive enabled long-life rechargeable aqueous zinc ion batteries. *Nano Energy* **62**, 275-281, doi:https://doi.org/10.1016/j.nanoen.2019.05.042 (2019).

4 Zeng, X. *et al.* Toward a Reversible Mn4+/Mn2+ Redox Reaction and Dendrite-Free Zn Anode in Near-Neutral Aqueous Zn/MnO2 Batteries via Salt Anion Chemistry. *Advanced Energy Materials* **10**, 1904163, doi:https://doi.org/10.1002/aenm.201904163 (2020).

5 Chen, Z. *et al.* Anion Solvation Reconfiguration Enables High-Voltage Carbonate Electrolytes for Stable Zn/Graphite Cells. *Angewandte Chemie International Edition* **59**, 21769-21777, doi:https://doi.org/10.1002/anie.202010423 (2020).

6 Zhang, C. *et al.* The electrolyte comprising more robust water and superhalides transforms Zn-metal anode reversibly and dendrite-free. *Carbon Energy* **3**, 339-348, doi:https://doi.org/10.1002/cey2.70 (2021).

7 Yang, W. *et al.* Hydrated Eutectic Electrolytes with Ligand-Oriented Solvation Shells for Long-Cycling Zinc-Organic Batteries. *Joule* **4**, 1557-1574, doi:https://doi.org/10.1016/j.joule.2020.05.018 (2020).

8 Hao, J. *et al.* Boosting Zinc Electrode Reversibility in Aqueous Electrolytes by Using Low-Cost Antisolvents. *Angewandte Chemie International Edition* **60**, 7366-7375, doi:https://doi.org/10.1002/anie.202016531 (2021).

9 Zeng, X. *et al.* Electrolyte Design for In Situ Construction of Highly Zn2+-Conductive Solid Electrolyte Interphase to Enable High-Performance Aqueous Zn-Ion Batteries under Practical Conditions. *Advanced Materials* **33**, 2007416, doi:https://doi.org/10.1002/adma.202007416 (2021).

10 Han, M. *et al.* Hydrated Eutectic Electrolyte with Ligand-Oriented Solvation Shell to Boost the Stability of Zinc Battery. *Advanced Functional Materials* **32**, 2110957, doi:https://doi.org/10.1002/adfm.202110957 (2022).

11 Han, D. *et al.* A non-flammable hydrous organic electrolyte for sustainable zinc batteries. *Nature Sustainability* **5**, 205-213, doi:10.1038/s41893-021-00800-9 (2022).

12 Wu, M. *et al.* A sustainable chitosan-zinc electrolyte for high-rate zinc-metal batteries. *Matter* **5**, 3402-3416, doi:https://doi.org/10.1016/j.matt.2022.07.015 (2022).

13 Jiang, H. *et al.* Chloride electrolyte enabled practical zinc metal battery with a near-unity Coulombic efficiency. *Nature Sustainability* **6**, 806-815, doi:10.1038/s41893-023-01092-x (2023).

14 Li, C. *et al.* Enabling selective zinc-ion intercalation by a eutectic electrolyte for practical anodeless zinc batteries. *Nature Communications* **14**, 3067, doi:10.1038/s41467-023-38460-2 (2023).

15 Dong, D., Wang, T., Sun, Y., Fan, J. & Lu, Y.-C. Hydrotropic solubilization of zinc acetates for sustainable aqueous battery electrolytes. *Nature Sustainability*, doi:10.1038/s41893-023-01172-y (2023).

16 Wang, F. *et al.* Highly reversible zinc metal anode for aqueous batteries. *Nature Materials* **17**, 543-549, doi:10.1038/s41563-018-0063-z (2018).
17 Qiu, H. *et al.* Zinc anode-compatible in-situ solid electrolyte interphase via cation solvation modulation. *Nature Communications* **10**, 5374, doi:10.1038/s41467-019-13436-3 (2019).
18 Zhao, J. *et al.* "Water-in-deep eutectic solvent" electrolytes enable zinc metal anodes for rechargeable aqueous batteries. *Nano Energy* **57**, 625-634, doi:https://doi.org/10.1016/j.nanoen.2018.12.086 (2019).
19 Jiang, H. *et al.* Zn Metal Anode with a Near-Unity Coulombic Efficiency for Prototype Zn Batteries. *Nature Sustainbility* (2023).
20 Yang, C. *et al.* All-temperature zinc batteries with high-entropy aqueous electrolyte. *Nature Sustainability* **6**, 325-335, doi:10.1038/s41893-022-01028-x (2023).